LUND UNIVERSITY

Fluorescence Lidar Multicolor Imaging of Vegetation

Edner, H; Johansson, Jonas; Svanberg, Sune; Wallinder, E

Link to publication

Total number of authors:
4

Fluorescence lidar multicolor imaging of vegetation

H. Edner, J. Johansson, S. Svanberg, and E. Wallinder

Multicolor imaging of vegetation fluorescence following laser excitation is reported for distances of 50 m. A mobile laser-radar system equipped with a Nd:YAG laser transmitter and a 40-cm-diameter telescope was utilized. The laser light was Raman shifted to 397 nm with pulse energies of ~30 mJ. An image-intensified CCD camera with a specially designed split-mirror Cassegrainian telescope was utilized for the simultaneous recording of fluorescence images of leaves and branches in four different spectral bands. Additionally, fluorescence spectra at selected points within the detection area were measured with an image-intensified diode array system. Image processing permits extraction of information related to the physiological status of the vegetation and might prove useful in forest decline research.

Introduction

In many regions of Europe, forests are subject to severe damage as a result of environmental influence. It is of considerable interest to be able to perform early detection and mapping of damaged vegetation. One possibility is to use reflectance spectroscopy, which is readily adaptable to satellite multispectral imagery.[1] Active remote sensing through the use of a transmitter can provide additional information.[2] The first reports on remotely detected chlorophyll fluorescence concerned algeal fluorescence.[3] Apart from chlorophyll fluorescence, a strong OH stretch water Raman signal and a nonspecific broad fluorescence referred to as Gelbstoff were reported. In these experiments one or more photomultipliers were used as detectors. Nd:YAG lasers and excimer lasers provided enough excitation pulse energy for airborne systems. Soon the same technique was utilized over land for the remote detection of fluorescence from trees, bushes, and grass.[4,5] Using an optical multi-channel analyzer (OMA) one could record the full fluorescence spectra,[6,7] still with a good signal-to-noise ratio. As one would expect, the far-field spectra were shown to coincide with near-field spectra.

Although chlorophyll fluorescence had already been known for many years, the first researcher to correlate chlorophyll fluorescence with the mechanism of photosynthesis was Kautsky.[8,9] He discovered that when a dark-adapted plant is suddenly exposed to light, the fluorescence exhibits a rapid (0.1-s) fluorescence increase followed by a slow (3-min) decrease to a steady-state level (F_S). The Kautsky kinetics can be understood as a time-dependent quenching of the fluorescence.[10–13] For a dark-adapted system, the photosystem I and photosystem II reaction centers are open. This means that all free electrons obtained in the reaction centers are accepted by the electron acceptors Q_A. The quenching is then significant, yielding a low fluorescence. As the Q_A acceptors are rapidly being reduced, this energy pathway is shut down with an increase of pigment fluorescence as a result. With the slow onset of the photosynthesis the electron acceptors are reoxidized and the electron transport gradually becomes more efficient, resulting in a lowered fluorescence. Additionally, if the photosynthetic pathways are blocked as a result of an external interference such as water stress, the Kautsky fluorescence kinetics is different. Furthermore, information about the photosynthetic status of stressed and normal plants can be obtained from the fluorescence spectrum.[11] As a result of partial overlap of a chlorophyll absorption band and the 685-nm fluorescence peak, the ratio of the two chlorophyll fluorescence peaks, I(685)/I(740), is dependent on fluorescence reabsorption, which is in turn chlorophyll-concentration dependent. Thus long-term stress of green plants can be monitored in terms of a higher I(685)/I(740) ratio as a result of a lowered chlorophyll concentration. Additionally, the blue fluorescence from other leaf chromophores, e.g., carotene, flavin adenine dinucleotide, nicotinamide ad-
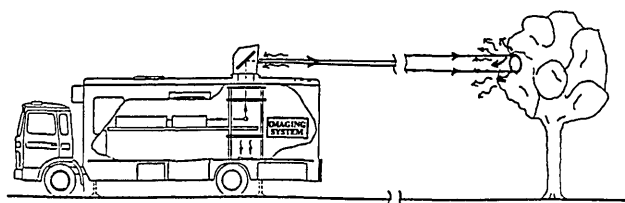
Fig. 1.   Remote fluorescence imaging of vegetation.

enine dinucleotide phosphate, and coumarin, may yield information about the plant condition.[14-18] The situation is, however, complicated by the fact that the fluorescence spectrum as well as the Kautsky kinetics are different for different plant species and also for different leaf structures.   The upper side of leaves exhibits a different fluorescence from the lower side,[19] and sun leaves have a different fluorescence than shadow leaves.   Therefore, it is important to use all fluorescence features that provide information about the plant.

In this paper we report on remotely recorded fluorescence images of different plants.   We also show how the spectral information can be maintained in the images by using a split-mirror telescope and

computer processing.   By the simultaneous recording of fluorescence images at selected wavelengths, spectral ratios such as I(685)/I(740) were calculated for each pixel, resulting in a false-color image showing the relative chlorophyll concentration.   Fluorescence spectra were separately recorded by using an OMA system.   Inserting a mirror in the optical pathway, we recorded the fluorescence spectra from selected spots in the whole image.   Preliminary results were reported at the 1992 Conference on Lasers and Electro-Optics.[20]

Instrumentation

Following remote spectral point monitoring of vegetation fluorescence[7] by using a mobile system intended primarily for atmospheric lidar investigations,[21] we performed remote fluorescence imaging of vegetation by using a multicolor imaging system[22] adapted to the 40-cm-diameter optical receiving telescope of the lidar system.   A view of this type of measurement is given in Fig. 1.   The laser transmitter of the lidar system is a Nd:YAG laser with frequency doubling or tripling.   The mobile lidar system originally uses a dye laser, pumped by the Nd:YAG laser.   The outgoing beam is directed coaxially with a vertically
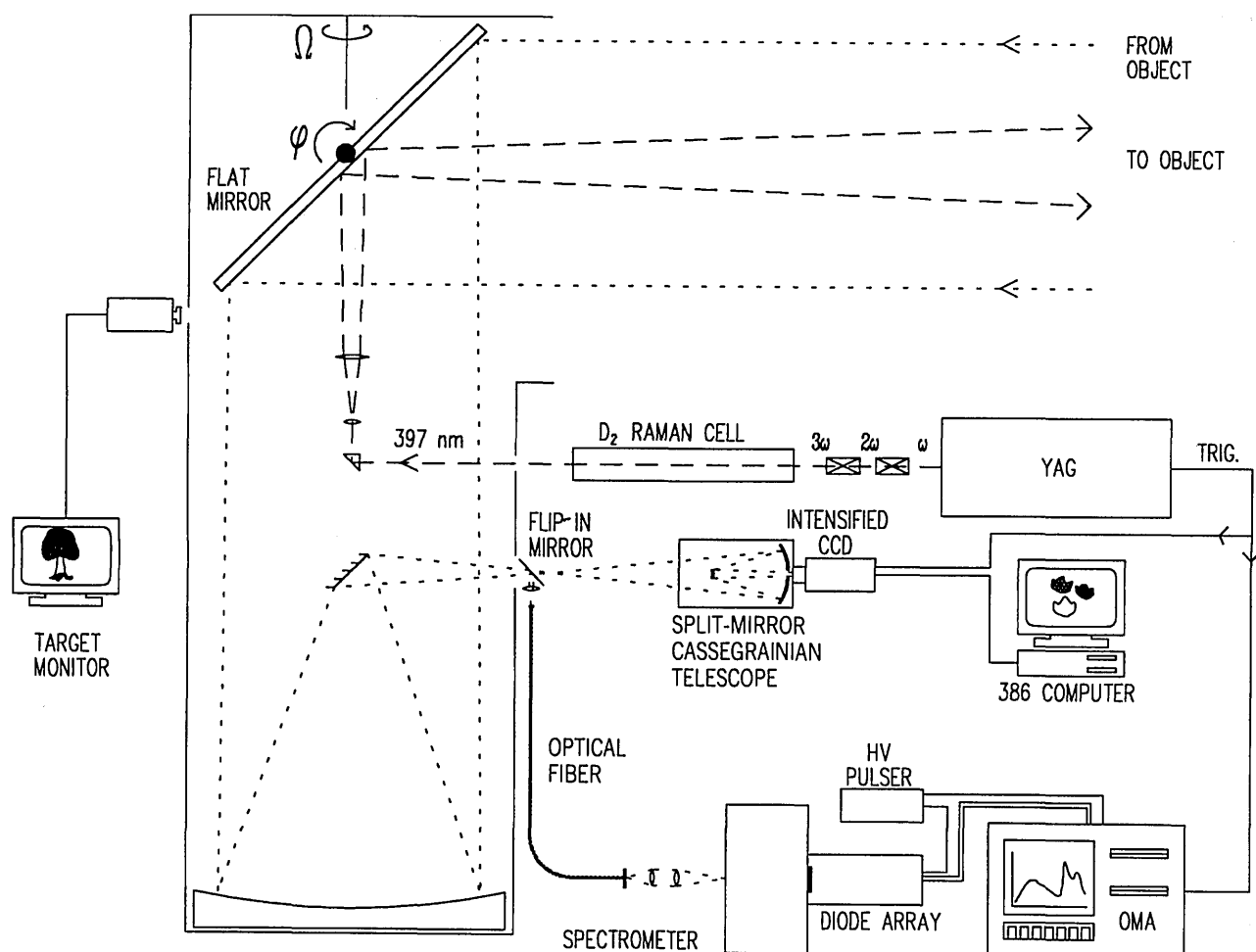

Fig. 2.   Optical and electronic layout of the multicolor fluorescence imaging system.   An OMA system for spectral recordings is included; HV, high voltage.

mounted 40-cm-diameter telescope and is transmitted toward the target by means of a large flat mirror in a retractable transmitting–receiving dome on the roof. Computer-controlled stepper motors are used to turn the dome and to tilt the mirror. A video camera is used to provide an image of the target area. When used in the field, the system is supplied with electric power from a 20-kW Diesel motor generator, which is housed in a trailer towed by a truck.

To induce chlorophyll fluorescence efficiently while still staying eyesafe, we made sure that the output from the frequency-tripled Nd:YAG laser (355 nm, 200-mJ pulse energy) was Raman shifted in a high-pressure deuterium cell to generate radiation at 397 nm. An output pulse energy of 30 mJ was achieved at 20 Hz. In the first studies a dye laser operating at 398 nm (Exalite 398 dye) was used instead of the Raman cell. The pulse energy was approximately the same, although the beam quality was much lower for the dye laser. Furthermore, the lifetime of the available laser dyes was very short. The radiation was transmitted in a divergent beam toward the target area. The fluorescence light was collected by the lidar telescope and directed into a second, Cassegrainian telescope as shown in Figs. 2 and 3. The image plane of the lidar telescope coincided with the object plane of the Cassegrainian telescope. In the image plane of the Cassegrainian telescope an image-intensified CCD camera (Delli Delti) was placed. The gate width of the image intensifier was set at 150 ns or less to suppress influence of the daylight illumination of the object efficiently. The image-intensified CCD camera was later replaced by a similar one (Spectroscopy Instruments Model ICCD-576). The Cassegrainian telescope has its first mirror cut into four segments that can be individually adjusted. By tilting the mirror segments, we found that each segment produces an image at the image intensifier; in total there are four identical images arranged as four quadrants on the detector. Furthermore, different interference filters or Schott colored-glass filters were placed before each mirror segment, matching specific features of the fluorescence spectra. Such features may include the broadband fluorescence structures at 450 and 520 nm and the chlorophyll fluorescence peaks at 685 and 740 nm, as further illustrated in Fig. 4. Alternatively, colored-glass filters can be used to select the broad blue-green spectral region or the overall red chlorophyll fluorescence. The fluorescence images are read out to an 8-bit frame-grabber board of a PC 386 computer. Computer processing makes it possible to generate a new image, pixel by pixel, from the four subimages by using a suitably designed spectral contrast function that enhances features of interest. The resulting image is shown on the screen in false color.

Alternatively, fluorescence could be collected point-wise and dispersed in an OMA. In this mode of operation a flip-in mirror was used in the optical pathway, guiding the fluorescence light into a 600-μm optical quartz fiber. The tip of the fiber was pierced through a white screen in the image plane of the lidar telescope in order to select a small, well-defined measurement area within the image more easily. The fluorescence light was guided through the optical fiber and lens coupled to an $f = 27$-cm Jarrel-Ash spectrometer. The detector was an image-intensified 1024-channel diode array from PARC (Model 1421). In this way remote fluorescence spectra were integrated over 500 laser pulses and displayed on the screen of the OMA mainframe (Model 1460). The gating pulse width was ~ 300 ns during the measurements.

Results

Spectra from green and slightly yellow maple leaves (*Acer platanoides*) at 50-m distance are included in Fig. 4 (lower left-hand corner). It can clearly be seen that, compared with the green leaf, the yellowish leaf exhibits a strong reduction in the 740-nm fluorescence peak in relation to the 690-nm peak. This is due to the lower chlorophyll content in the yellowish leaf.[11] In addition, the blue-green fluorescence is somewhat different for the two leaves, with an enhanced peak at 520 nm for the yellowish leaf. Spatially resolved recordings of the same leaves are shown in the upper half of the figure, with images recorded at 690, 740, 450, and 397 nm, respectively. The subimage at 397 nm showing the elastically scattered laser light contains virtually no information because of the specular reflection of the unidirectionally incoming light. The subimages at 450, 690, and 740 nm show the spatial distribution of the fluorescence from the leaves. This is, however, strongly
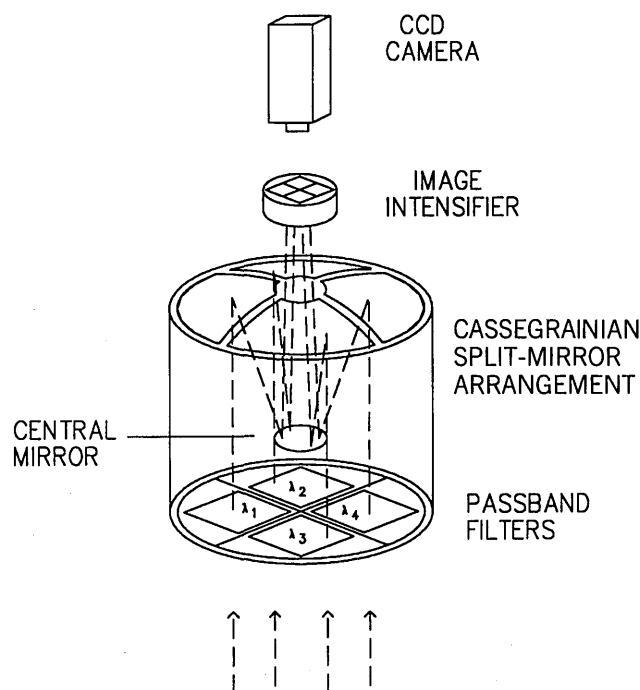

Fig. 3. Cassegrainian telescope attached to an image-intensified CCD camera. The first mirror is split into four segments, with optical filters placed in front of each segment.
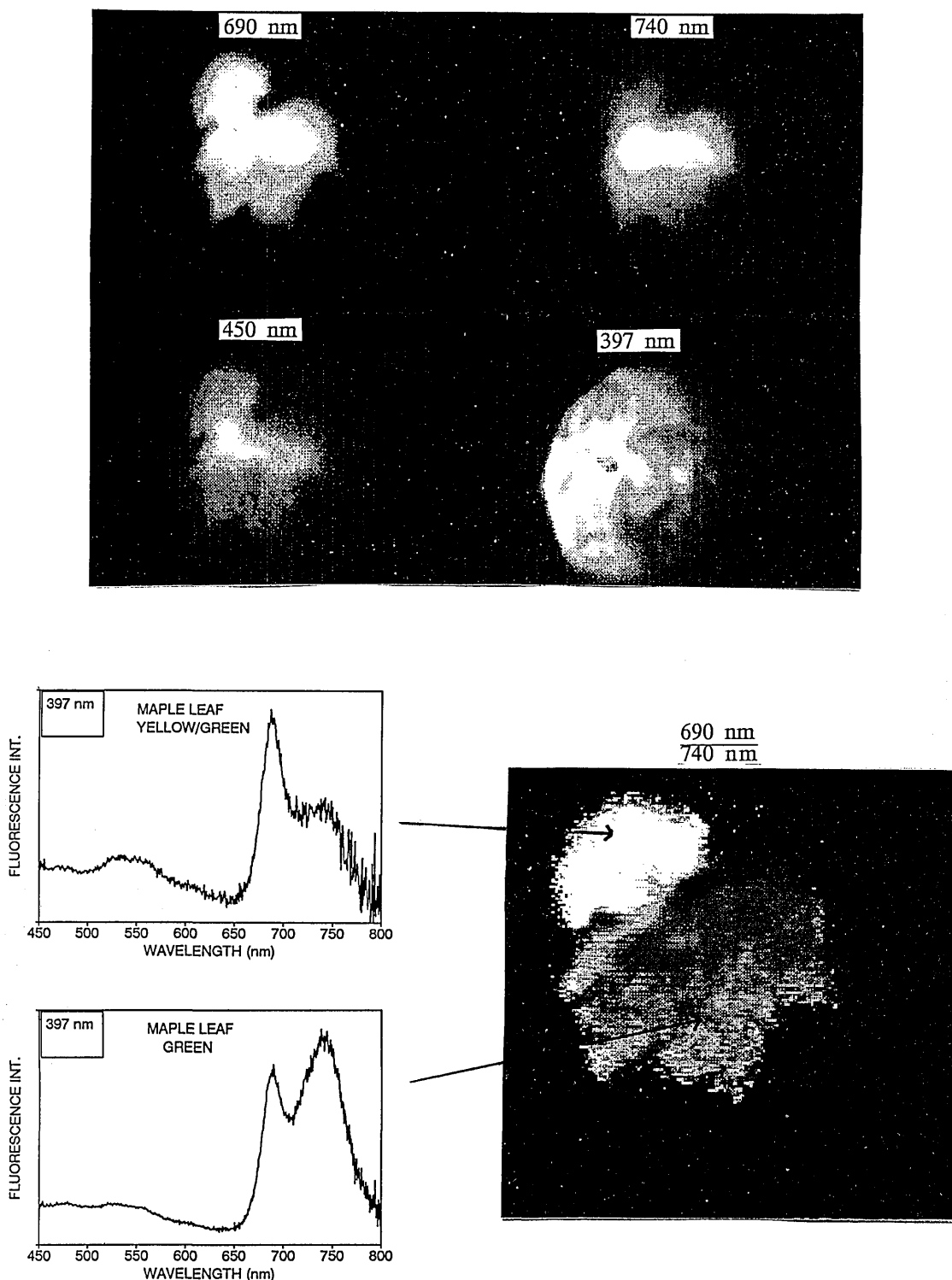
Fig. 4. Simultaneous fluorescence images of two maple leaves (*Acer platanoides*) recorded at 690, 740, and 450 nm. An elastic backscattering image is also seen. A computer-processed image obtained by dividing the 690- and 740-nm subimages is shown, clearly discriminating between a green and a slightly yellow leaf. Fluorescence spectra from the same green and slightly yellow leaves recorded at a 50-m distance are included and clearly show the origin of the discrimination.

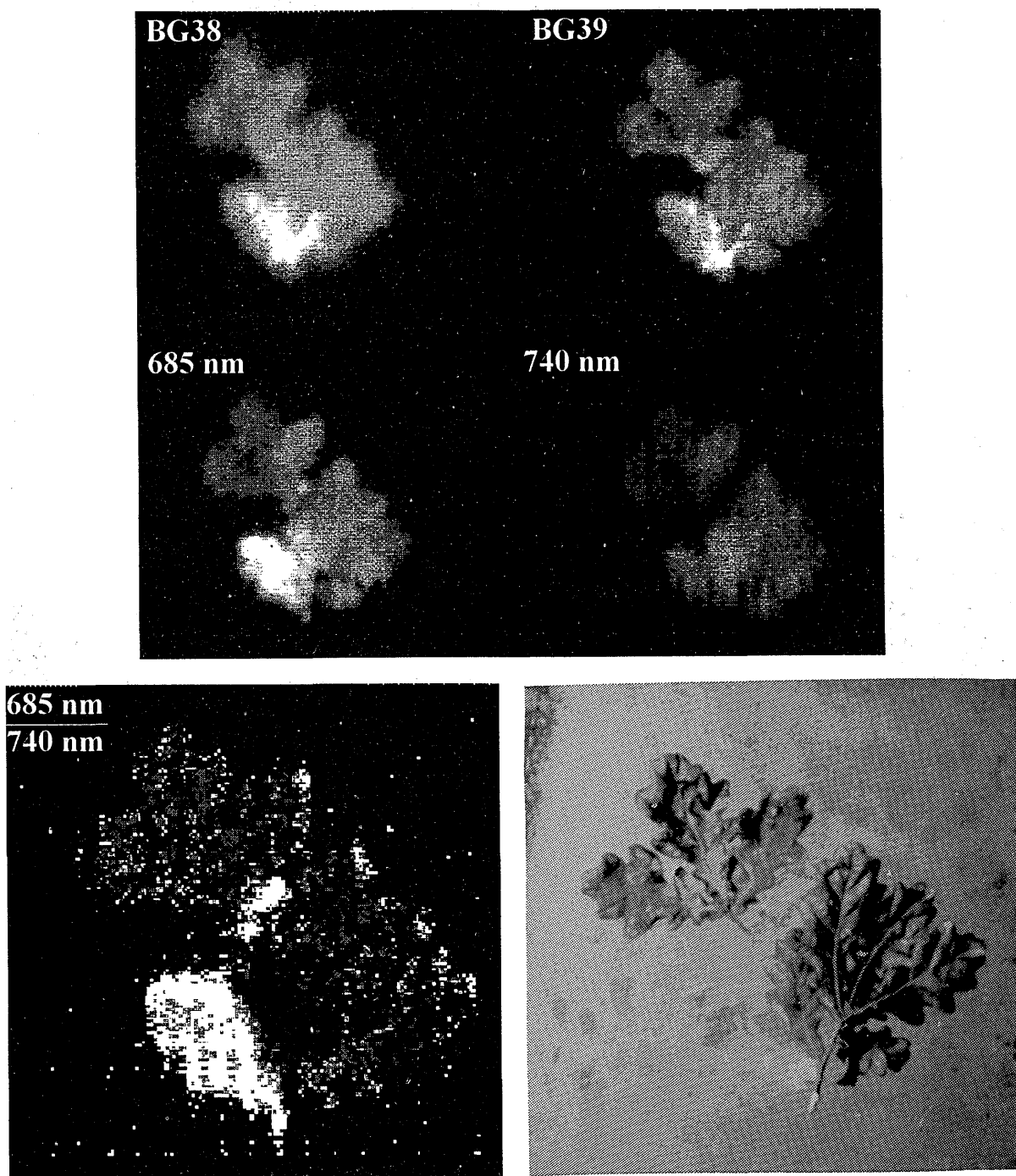Fig. 5. Simultaneous fluorescence images recorded with BG38 and BG39 Schott colored-glass filters as well as 685- and 740-nm interference filters. The object is a branch of 10 oak leaves (*Quercus robur*) situated at a distance of 50 m. A processed image showing the ratio of the fluorescence obtained by using 685-nm and 740-nm interference filters is shown in the lower left-hand corner. A photograph of the scene is shown in the lower right-hand corner. The leaf at the lower left in the photograph and a small one in the middle are yellowish.

affected by the excitation beam profile, which makes the separate subimages difficult to interpret. To exemplify image processing for extracting environmental information, we show an image obtained by dividing the 690-nm image by the 740-nm image, pixel by pixel. This is a simple example of the use of a spectral contrast function. In the resulting image (lower right-hand corner), the leaf with the lower chlorophyll content, the yellowish one, is strongly demarcated against the normal green leaf. The pixel values for the yellowish leaf were approximately twice as high as those for the green leaf. Furthermore, the edges of the green leaf show a slightly higher value, possibly indicating a beginning autumnal senescence.
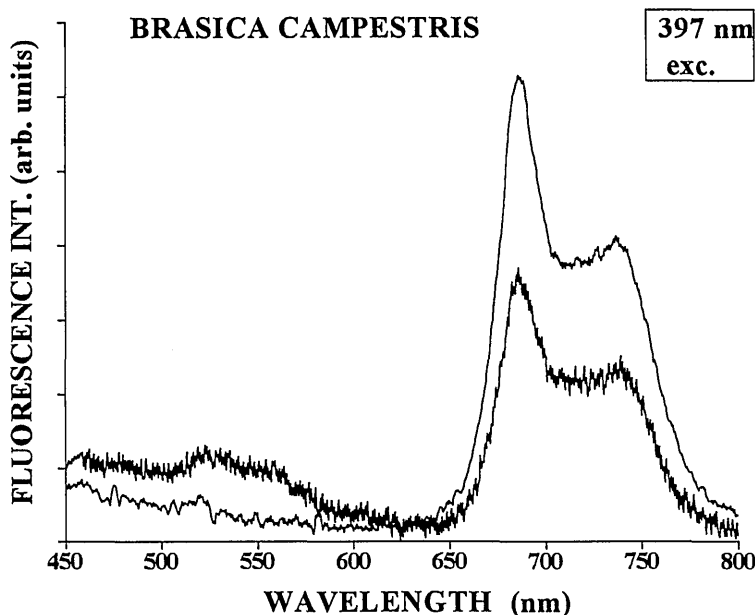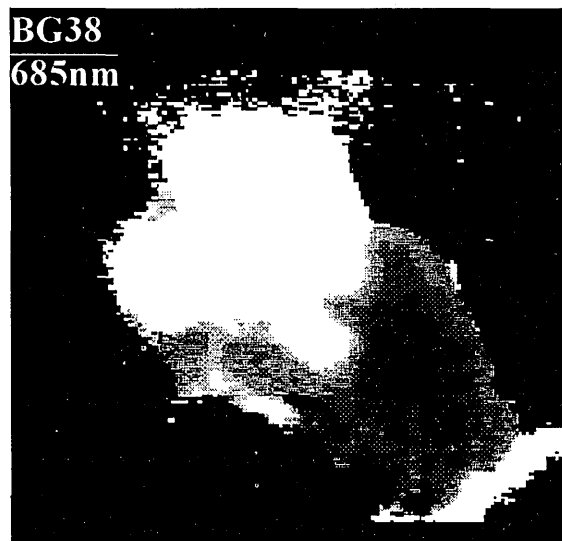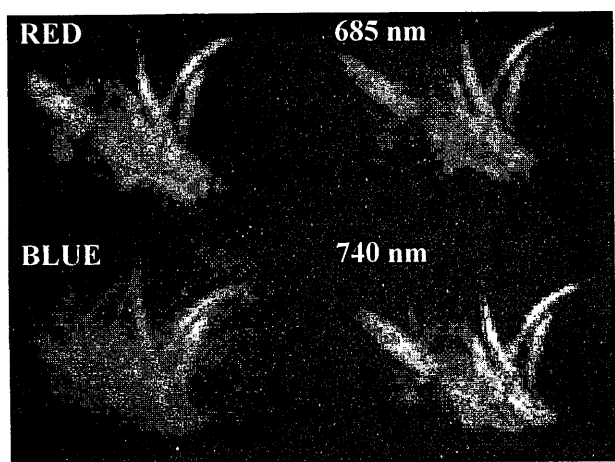
Fig. 6. Two leaves of *Brasica campestris* (upper left-hand corner) grown in normal light and in the presence of additional UV light. The leaf to the left is exposed to UV light. A false-color image was formed dividing the blue fluorescence by the red fluorescence pixel by pixel (upper right-hand corner). The corresponding optical filters were Schott BG38 and a 685-nm interference filter, respectively. Below are two fluorescence spectra remotely recorded for each of the two leaves.

As can be seen from the processed image (lower right-hand corner), the beam-profile artifact has now disappeared as a result of the division of one image by another. Thus by displaying the ratio of two signals rather than the intensity at one wavelength, we have obtained not only an enhanced demarcation but also an image that is independent of the beam profile. This is a particularly important aspect for remote fluorescence recordings. Similar measurements were also performed on a branch of oak (*Quercus robur*) including 10 leaves, two of which were yellowish as a result of the beginning senescence. The fluores-

cence was measured at 685 and 740 nm as well as in the blue region through Schott BG38 and BG39 colored-glass filters (>50% transmission from 350 to 600 nm). The fluorescence images in the four spectral bands and a processed image showing the ratio of the fluorescence through the 685- and 740-nm filters are shown in Fig. 5. A photograph of the scene is also included in Fig. 5. As we can see, the two yellowish leaves, one partially covered, are clearly visualized in the processed image by their higher ratio.
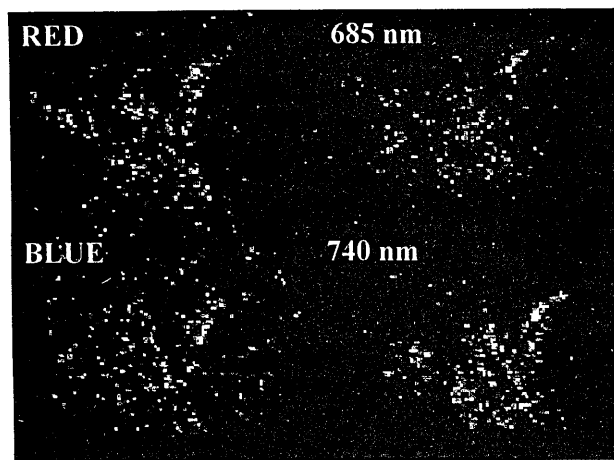
Experiments were also made on leaves of *Brasica*

RED   685 nm

BLUE   740 nm

100 pulses

RED   685 nm

BLUE   740 nm

20 pulses

RED   685 nm

BLUE   740 nm
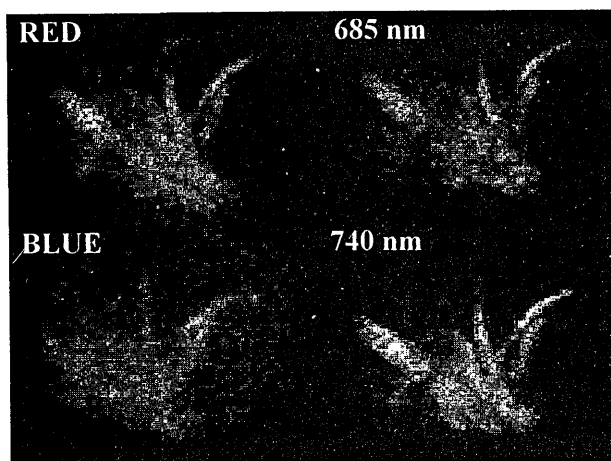
1 pulse

Fig. 7. Three sets of multicolor fluorescence images of a maize plant recorded by using 100, 20, and 1 laser pulses, respectively. The filters chosen were 685- and 740-nm interference filters and Schott BG7 (blue) and GG645 (red) colored-glass filters. The target distance was 40 m and the excitation wavelength was 397 nm.

campestris, as shown in Fig. 6 (upper left-hand corner). Normal plants were compared with plants subject to enhanced UV radiation (ozone-hole simulation). The fluorescence was recorded by using inter-
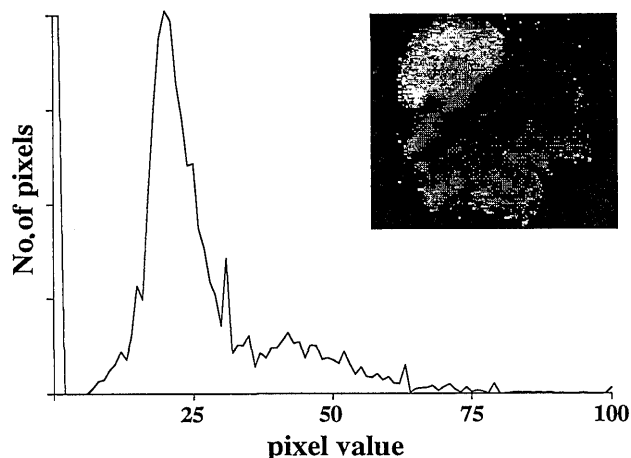

Fig. 8. Diagram showing the distribution of pixel values of the processed image in Fig. 4 (inserted image).

ference filters of 685, 740, and 470 nm as well as a Schott BG38 colored-glass filter. The discrimination was provided in the red-to-blue ratio, as shown in the remotely recorded fluorescence spectra included in Fig. 6 (bottom half). In the upper right-hand corner of this figure, a processed image obtained by dividing the blue intensity by the red intensity is also presented. The UV-damaged leaf, the one to the left, has the higher blue-to-red ratio.

An important issue is the signal-to-noise characteristics of the recording system. The signal-to-noise ratio has to be high enough to yield a reasonable image of the object. Moreover, the recorded multicolor image must have a sufficient signal-to-noise ratio value to permit computer processing, e.g., division of one subimage by another, and still give a true image of the object. Furthermore, a future airborne system has to operate on a single-shot basis. The movement of an aircraft does not permit integration that would enhance the signal-to-noise ratio. Figure 7 shows three sets of multicolor images of the same object, a maize plant, obtained from the integration of 100, 20, and 1 laser shots. The object had a diameter of ~40 cm. A comparison of the images shows that with the present system an integration of ~20 laser shots is necessary to obtain a useful signal-to-noise ratio value.

The detector noise level is a limiting factor in obtaining high-quality images. Other factors that result in intensity variations in an image are scattered sunlight and the natural variation of the fluorescence over an inhomogeneous object. The gate width was set to ~150 ns, and on some occasions when the sunlight was falling directly on the object a gate width of as short as 6–8 ns could be used. Nevertheless, a small portion of sunlight was able to reach the detector during the short gate and had to be subtracted as a background. For cases of a high background level, the subtraction added noise to the detector noise. Moreover, the true spectral variations of the fluorescence for different locations over a leaf are substantial. This results in variations of the

fluorescence ratio displayed in the processed image. These data variations induced by the detection system as well as the natural variations are illustrated in Fig. 8, for the maple leaves of Fig. 4. A diagram of the occurrence of the different pixel values within the processed image (the inserted image) is shown. The diagram shows two peaks at the pixel values (or gray levels) 20 and 40, corresponding to the two leaves. Additionally, a strong peak (truncated) at values between 0 and 3 represents the black background of the image. The peak at level 20, which is the green leaf, corresponds to a fluorescence ratio of 0.85. The FWHM was estimated to be ~0.3 on a fluorescence ratio scale. The peak at level 40, the yellowish leaf, corresponds to a fluorescence ratio of 1.77. The FWHM was difficult to calculate for this peak because it is partially covered by the other peak but is at least much broader. This is what one would expect, because this peak represents different stages of senescence within the leaf, whereas the green leaf can be expected to have a normal concentration of chlorophyll in the entire leaf.

Discussion

Point measurements of fluorescence from green plants have shown that information on the physiological state can be obtained. The ratio of the two red chlorophyll peaks correlates well with the amount of chlorophyll in the leaves and also the red-to-blue ratio changes with the plant condition.[11] The red-to-blue ratio has also been shown here to change in plants subject to strong UV irradiation. The origin of the enhanced blue fluorescence from the UV-damaged leaves is not clear. One possibility is that the strong UV radiation has caused bond breaking in the fluorophores and thereby has changed the fluorescence properties of the fluorophores.

It is desirable to perform fluorescence measurements not only in a point monitoring mode but in full images. However, fluorescence images at one selected wavelength, such as shown in the upper part of Fig. 4, are difficult to interpret. A lowered red fluorescence intensity at a certain location in the target area does not necessarily mean a low chlorophyll content, because the detected signal depends not only on chromophore concentration but also on excitation intensity and target distance. A dimensionless ratio, in contrast, is not sensitive to variations of such parameters and is therefore better suited for fluorescence measurements of plants. A comparison of the individual subimages versus the processed image in Fig. 4 clearly shows the advantage of displaying the ratio. From the subimages one can see a hot spot from the laser in the center of each subimage. In the case of the processed image, this has disappeared as a result of the ratioing.

To gain full advantage of a dimensionless ratio, one must record the fluorescence subimages at the different wavelengths simultaneously, all of them excited by the same laser pulse. Otherwise errors will be induced by movements of the target and pulse-to-pulse fluctuations of the laser. This rules out a system for sequential acquisition at the different wavelengths. By using a split-mirror telescope, as illustrated in this paper, we record the fluorescence images simultaneously at the different wavelengths. From the subsequent computer processing we can condense the spectral information in the four individually filtered images into one image, displaying the pixel values by using a spectral demarcation function that obtains its input values from the individual image pixels. In principle, the design with the split-mirror telescope permits single-shot image detection of plant physiological status. A statistical analysis of multileaf frames will be performed within the European LASFLEUR project, aiming at early airborne detection of forest decline.

References

1. B. N. Rock, J. E. Vogelmann, D. L. Williams, A. F. Vogelmann, and T. Hoshizaki, "Remote detection of forest damage," BioScience 36, 439–445 (1986).
2. L. Pantani and R. Reuter, eds., feature on lidar in remote sensing of land and sea, Adv. Remote Sensing 1(2) (1992).
3. F. E. Hoge and R. N. Swift, "Airborne simultaneous spectroscopic detection of laser-induced water Raman backscatter and fluorescence from chlorophyll a and other naturally occurring pigments," Appl. Opt. 20, 3197–3205 (1981).
4. F. E. Hoge, R. N. Swift, and J. K. Yungel, "Feasibility of airborne detection of laser-induced fluorescence emission from green terrestrial plants," Appl. Opt. 22, 2991–3000 (1983).
5. R. Zimmermann and K. P. Günther, "Laser-induced chlorophyll-a fluorescence of terrestrial plants," in International Geoscience and Remote Sensing Symposium IGARSS'86 (ESA Publications, Nordwijk, The Netherlands, 1986), pp. 1609–1613.
6. A. Rosema, G. Cecchi, L. Pantani, B. Radicati, M. Romuli, P. Mazzinghi, O. van Kooten, and C. Kliffen, "Results of the 'LIFT' project: air pollution effects on the fluorescence of Douglas fir and poplar," in Applications of Chlorophyll Fluorescence, H. K. Lichtenthaler, ed. (Kluwer, Dordrecht, The Netherlands, 1988).
7. H. Edner, J. Johansson, S. Svanberg, E. Wallinder, M. Bazzani, B. Breschi, G. Cecchi, L. Pantani, B. Radicati, V. Raimondi, D. Tirelli, G. Valmori, and P. Mazzinghi, "Laser-induced fluorescence monitoring of vegetation in Tuscany," EARSeL Adv. Remote Sensing, 1, 119–130 (1992).
8. H. Kautsky and A. Hirsch, "Neue Versuche zur Kohlenstoffassimilation," Naturwissenschaften 19, 964 (1931).
9. H. Kautsky and U. Franck, "Chlorophyllfluoreszenz und Kohlensäureassimilation," Biochem Z. 315, 139–155 (1943).
10. P. Mohanthy and Govindjee, "The slow decline and the subsequent rise of chlorophyll fluorescence transients in intact algeal cells," Plant Biochim J. 1, 78–106 (1974).
11. H. K. Lichtenthaler and U. Rinderle, "The role of chlorophyll fluorescence in the detection of stress conditions in plants," CRC Crit. Rev. Anal. Chem. 19, S29–S85 (1988).
12. H. K. Lichtenthaler, C. Bauschmann, U. Rinderle, and G. Schmuck, "Application of chlorophyll fluorescence in ecophysiology," Radiat. Environ. Biophys. 25, 297–308 (1986).
13. G. H. Krause and E. Weis, "Chlorophyll fluorescence as a tool in plant physiology. II. Interpretation of fluorescence signals," Photosynth. Res. 5, 139–157 (1984).

14. L. Celander, K. Fredriksson, B. Galle, and S. Svanberg, "Investigation of laser-induced fluorescence with applications to remote sensing of environmental parameters," Rep. GIPR-149 (Göteborg Institute of Physics Reports, Göteborg, Sweden, 1978); S. Svanberg, "Laser fluorescence spectroscopy in environmental science," in *Optoelectronics for Environmental Science,* S. Martellucci and A. N. Chester, eds. (Plenum, New York, 1989), pp. 15–27.

15. L. N. M. Duysens and G. Sweep, "Fluorescence spectrophotometry of pyridine nucleotide in photosynthesizing cells," Biochim. Biophys. Acta **25,** 13–16 (1957).

16. E. W. Chappelle, F. M. Wood, Jr., J. E. McMurtrey III, and W. Newcomb, "Laser-induced fluorescence of green plants. 1: A technique for the remote detection of plant stress and species differentiation," Appl. Opt. **23,** 134–138 (1984).

17. H. K. Lichtenthaler, "Chlorophylls and carotenoids: pigments of photosynthetic biomembranes," Methods Enzymol. **148,** 350–382 (1987).

18. Y. Goulas, I. Moya, and G. Schmuck, "Time-resolved spectroscopy of the blue fluorescence of spinach leaves," Photosynth. Res. **25,** 299–307 (1990).

19. U. Schreiber, R. Fink, and W. Vidaver, "Fluorescence induction in whole leaves: differentiation between the two leaf sides and adaption to different light regimes," Planta **133,** 121–129 (1977).

20. H. Edner, J. Johansson, S. Svanberg, and E. Wallinder, "Remote multicolor imaging of vegetation laser-induced fluorescence," in *Conference on Lasers and Electro-Optics,* Vol. 12 of 1992 OSA Technical Digest Series (Optical Society of America, Washington, D.C., 1992), pp. 432–433.

21. H. Edner, K. Fredriksson, A. Sunesson, S. Svanberg, L. Unéus, and W. Wendt, "Mobile remote sensing system for atmospheric monitoring," Appl. Opt. **26,** 4330–4338 (1987).

22. P. S. Andersson, S. Montán, and S. Svanberg, "Multi-spectral system for medical fluorescence imaging," IEEE J. Quantum Electron. **QE-23,** 1798–1805 (1987).